



OPEN A novel method for estimating functional connectivity from EEG coherence potentials

Narayan Puthanmadam Subramaniyam^{1,2✉} & Tara C. Thiagarajan¹

Analysis of functional connectivity can provide insights into how the brain performs various cognitive and behavioral tasks as well as the neural mechanisms underlying several pathologies. In this work, we describe a novel approach to estimate functional connectivity from electroencephalography (EEG) data using the concept of coherence potentials (CPs), which are defined as clusters of high-amplitude deflections with similar waveform shapes. We define connectivity measures based on features of CPs, including the time intervals between CP peaks and their co-occurrence on different electrodes or channels. We used EEG data from 25 healthy subjects performing three tasks - resting state (eyes closed and eyes open), working memory and pattern completion tasks to investigate the ability of CP based connectivity measures to distinguish between these tasks. When compared with traditional connectivity measures including several spectral-based measures and mutual information, our results showed that CP based connectivity measures more robustly and significantly distinguished between all the tasks both at group-level and subject-level. In conclusion, CP based EEG connectivity measures provide a reliable way to distinguish between different cognitive task conditions and could pave way in the early detection of neurological disorders such as Alzheimer's disease that affect various cognitive tasks.

Functional connectivity refers to statistical interdependencies between the functional properties of different brain regions and is used to describe the interaction between brain regions¹. Functional properties can be measured in various ways using different neuroimaging modalities, such as electroencephalography (EEG), magnetoencephalography (MEG), functional magnetic resonance imaging (fMRI) or near-infrared spectroscopy. Studying functional connectivity can provide insights into how different regions of the brain communicate and work together to perform various cognitive and behavioral functions^{2,3}. Studying functional connectivity can also be helpful in understanding the underlying neural mechanisms of various brain disorders, including autism spectrum disorder⁴, Alzheimer's disease⁵ and epilepsy⁶ to mention a few. Furthermore, functional connectivity has also been used in brain-computer interface applications for example, to decode motor intention⁷ and in emotion recognition⁸.

Among these neuroimaging modalities, EEG is inexpensive, portable, easily accessible across the world, and it has millisecond-level temporal resolution, making it an optimal (and often the only feasible) choice for studying functional connectivity in routine clinical applications, ambulatory settings and naturalistic environments.

Several methods to estimate functional connectivity from EEG data have been developed^{2,3,9}, including simple linear correlation, spectral, and information-theoretic approaches. Spectral-based approaches such as coherence¹⁰, phase locking value¹¹, phase-lag index¹², imaginary coherence¹³ and multivariate auto-regressive (MVAR) methods^{14–16} estimate the relationship between EEG time series using the cross-spectral density matrix. Information-theoretic approaches such as mutual information¹⁷, transfer entropy¹⁸ and ordinal partition transition networks¹⁹ have also been used to estimate functional connectivity from electrophysiological time series. These measures estimate the amount of information one signal contains about another signal in terms of marginal and conditional entropies²⁰.

Functional connectivity can be further categorized into bivariate and multivariate measures². Bivariate approaches estimate only pairwise interactions. Examples of bivariate approaches include coherence, mutual information, phase locking value, phase-lag index, and transfer entropy. In contrast, multivariate approaches also take into account the effects of confounders. These approaches include MVAR approaches, ordinal partition networks, and multivariate transfer entropy. Furthermore, these connectivity metrics can be symmetric, meaning the metric only gives information about the connectivity between two brain regions or electrodes, with no information on the direction of interaction (e.g., phase locking value, coherence, imaginary coherence,

¹Sapien Labs, 1201 Wilson Blvd, Arlington 22209, VA, USA. ²Faculty of Medicine and Health Technology, Tampere University, 33520 Tampere, Finland. ✉email: narayan@sapienlabs.org

mutual information) or asymmetric, where the direction of interaction between two brain regions or electrodes can also be established (e.g., MVAR, transfer entropy, phase lag index).

The aforementioned methods of estimating functional connectivity focus on statistical relationships of different aspects of the signal (for example, phase or amount of information). However, it is not always known *a priori* which aspect of statistical dependence or interplay is most relevant in distinguishing brain states, for e.g., between different task conditions or between healthy and diseased population. Thus exploration of new methods can potentially provide insight into the structures and patterns of the signals that are of relevance for different tasks and brain states.

In this work, we propose a new method to estimate functional connectivity (symmetric and bivariate) between EEG signals. The proposed method draws from an earlier work on organotypic cortex slices (in vitro) and in microelectrode arrays implanted in the monkey cortex, which shows that local field potentials are able to propagate across the cortex without distortion to their shape when they exceed a certain amplitude threshold²¹. These clusters of high-amplitude potentials of highly correlated waveforms have been called coherence potentials (CPs). This suggests that the structure of these high amplitude potentials may carry information that is more pertinent to task processing than the entirety of the signal. As a preliminary demonstration of this possibility, studies in human electrocorticography (ECoG) have shown that CP of a particular waveform originating in the finger representation area of the cortex predict the reaction time on a fist clenching task²². Here we show that coherence potentials, defined as clusters of high amplitude correlated waveforms exist in EEG despite volume conduction of the skull, and characterize connectivity based on their spatiotemporal structure to see if they carry meaningful information about task conditions. We define novel connectivity measures based on various features derived from CPs.

We used four task conditions - resting eyes closed (EC), resting eyes open (EO), performance of a working memory (WM) task and performance of a Raven's progressive matrix pattern completion (PC) task. Since our metric is bivariate and symmetric, we contrast these coherence potentials connectivity measures with other bivariate and symmetric estimations of connectivity that utilize aspects of the entire signal or specific spectral components of the signal, such as absolute coherence (*absCoh*), phase locking value (*PLV*), imaginary part of coherence (*imCoh*) or mutual information (*MI*), demonstrating a relatively better ability to distinguish among these tasks. Fundamentally this method contrasts to other methods in that it assumes that it is the waveform shape of high amplitude periods that represent the important component of the signal for information transfer rather than a particular spectral component or characteristic.

Materials and methods

Ethical statement

This study was approved by the Health Media IRB (USA, OHRP IRB #00001211) and Sigma-IRB (India) and this study is conducted in accordance with Title 45, the code of federal regulations, sub-part A of NIH (USA), and Indian Independent Ethics Committee requirements. All the participants provided the informed consent.

Experimental conditions and EEG data acquisition

We used EEG data recorded from 25 subjects for 3 minutes under four different experimental conditions^{23,24} - 1) Eyes Closed (EC) 2) Eyes Open (EO) 3) Pattern Completion (PC) and 4) Working Memory (WM). For the EC condition, the participants were instructed to relax with eyes closed. For the EO condition, the participants were instructed to have their eyes open and look at images on a laptop screen. The WM task involved iteratively retracing a pattern on a grid starting with a three dot pattern which increased in difficulty until the subject failed. The PC task utilized a Raven's progressive matrix which consisted of five questions related to pattern recognition, each in order of increasing difficulty and was administered using paper and pencil²³. The EEG data recorded ranged from 2.5 to 3 minutes for each of the tasks.

EEG recordings were performed using the Emotiv EPOC system with channels AF3, AF4, F3, F4, F7, F8, FC5, FC6, T7, T8, P7, P8, O1 and O2. The EEG signals were high-pass-filtered with a 0.16 Hz cutoff, pre-amplified, and low-pass-filtered at an 83 Hz cutoff. The analog signals were then digitized at 2048 Hz and filtered using a 5th-order sinc notch filter (50 and 60 Hz) before being down-sampled to 128 Hz (company communication). We further low-pass filtered the EEG signals to 40 Hz for further analysis.

Connectivity measures based on coherence potentials

Extraction of events

Periods of deflections from the baseline where the peak exceeded a threshold were extracted as events. For each subject, this threshold was chosen to be two times the average standard deviation ($\bar{\sigma}$) of EEG data (across 14 electrodes) from the baseline in the EC condition, which is used as the reference condition. The value $2\bar{\sigma}$ represents a threshold where events are not likely to be noise and are in the range of thresholds where coherence potential activity has been shown in LFPs and ECoG^{21,22}. In contrast to local field potentials recorded from cortex, where negative periods of large amplitudes dominate²⁵, in scalp EEG both positive and negative deflections are generally equivalent. Thus, for each EEG electrode, both positive and negative periods of signal deflections exceeding the threshold were extracted. Figure 1 (a) shows an example of EEG data from two electrodes (F3 and FC5) with periods of positive and negative deflections that cross the threshold ($\pm 2\bar{\sigma}$). Four large amplitude negative deflections are detected on FC3 and FC5 while one large amplitude positive deflection is detected on FC3.

Correlation as a measure of event similarity

Figure 1 (b) show the steps involved in computing the correlation between two events (positive or negative) crossing the threshold, which serves as a measure of the similarity of the waveform shape. The waveform

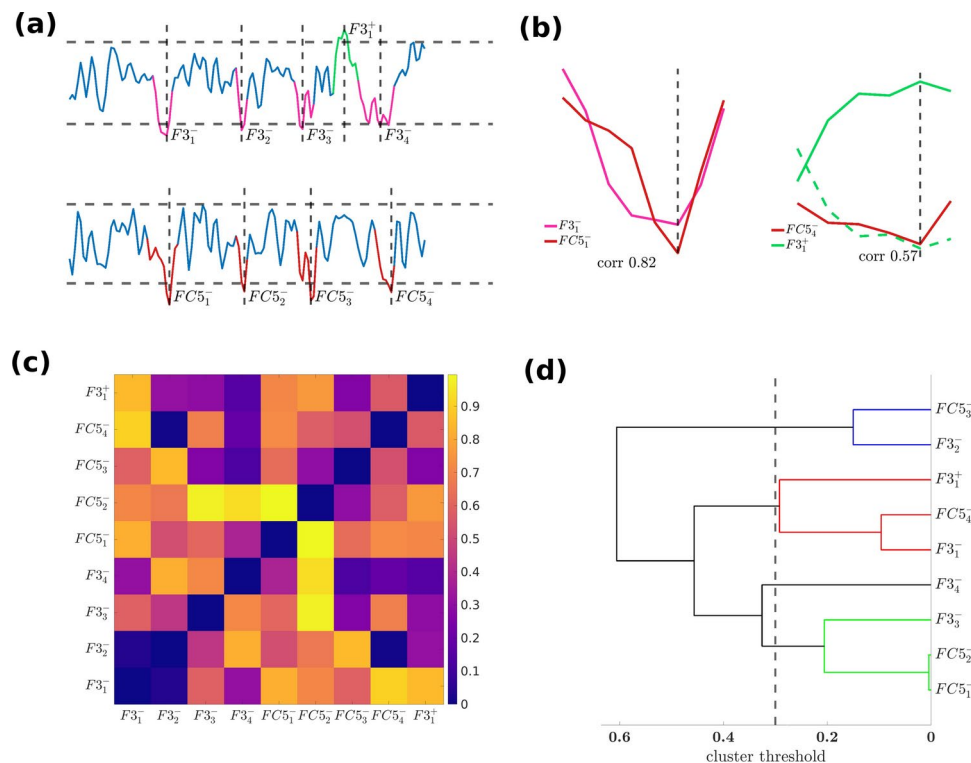


Fig. 1. Illustration of event extraction and computation of event similarity from EEG signals. **(a)** Example of two EEG signals from channels F3 and FC5. The threshold of 2σ is shown as a dotted horizontal line. Nine events that include both negative and positive deflections are detected on the two channels based on this threshold. **(b)** shows correlation computed between two negative events $F3_1^-$ and $FC5_1^-$ and between positive and negative events $F3_1^+$ and $FC5_4^-$. Note that in the sign of event $F3_1^+$ is flipped before computing the correlation. **(c)** The correlation matrix derived from nine events shown in (a). **(d)** Dendrogram showing the events partitioned into four clusters for a distance threshold of 0.3

similarity between two events is computed using a simple correlation metric after aligning the peaks of the two signals (vertical dashed lines) as shown in 1 (b). Where the events are of different lengths to the left and right of the peak, the signal period equivalent to the longer event is used. Figure 1 (b) also shows a scenario where correlation is computed to estimate the similarity between a positive and a negative deflection ($F3_1^+$ and $FC5_4^-$). In this case, before calculating the correlation the sign of one of the waveforms is flipped so that only the similarity in the waveform shape is considered, discarding the sign of deflection. Given that there are M such events (i.e., positive or negative deflections crossing 2σ) across all the electrodes, we form a correlation matrix $R \in \mathbb{R}^{M \times M}$. For the purpose of visualization, a 9×9 correlation matrix containing similarity between the nine signal deflections is shown in Figure 1 (c).

Hierarchical clustering

After computing the correlation matrix R , we clustered the events using agglomerative hierarchical clustering²⁶ based on a distance matrix defined as,

$$D = \mathbb{I} - R \quad (1)$$

where \mathbb{I} is a $M \times M$ identity matrix, with M representing the total number of events occurring on all the electrodes. Thus the distance value for each entry in the matrix is expressed as one minus the correlation coefficient. We used the average linkage method to calculate the distance between the clusters as the average linkage method had the highest cophenetic correlation compared to other linkage methods. We then varied the distance threshold between 0.1 to 0.8 in steps of 0.1 to visualize behavior at different thresholds. In the example shown in Figure 1, after obtaining the correlation matrix for 9 events (Figure 1 (c)), hierarchical clustering at a distance threshold of 0.3 results in four clusters represented by three colors (green, red, blue and black) as shown in Figure 1 (d).

Connectivity measures

We define the following connectivity measures between each pair of electrodes within each event cluster of CPs,

1. Mean inter-event interval, CP_τ
2. Maximum inter-event interval, $CP_{\tau_{max}}$

3. Minimum inter-event interval, $CP_{\tau_{min}}$
4. Connection frequency, CP_{λ}

The measures CP_{τ} , $CP_{\tau_{max}}$ and $CP_{\tau_{min}}$ are based on the event peak times. If there are $N_{i,p}$ and $N_{j,p}$ events on electrodes i and j in cluster p , then the inter event interval between electrodes i and j in cluster p is computed as,

$$CP_{\tau^p} = \frac{1}{N_{i,p}N_{j,p}} \sum_{n=1}^{N_{i,p}} \sum_{m=1}^{N_{j,p}} |t_i^m - t_j^n| \quad (2)$$

where t_i^m and t_j^n are the peak times (in seconds) of events m and n on electrodes i and j respectively.

The mean interaction measure CP_{τ} between electrodes i and j is given as,

$$CP_{\tau} = \frac{1}{P'} \sum_{p=1}^{P'} CP_{\tau^p} \quad (3)$$

where P is the total number of clusters and P' be the number of clusters clusters that contain events from electrodes i and j , i.e., $P' \subset P$. Similarly, for cluster p we compute $CP_{\tau_{min}^p}$ and $CP_{\tau_{max}^p}$ as,

$$CP_{\tau_{min}^p} = \min \left\{ |t_i^m - t_j^n| \mid \begin{array}{l} m = 1, \dots, N_{i,p}, \\ n = 1, \dots, N_{j,p} \end{array} \right\} \quad (4)$$

$$CP_{\tau_{max}^p} = \max \left\{ |t_i^m - t_j^n| \mid \begin{array}{l} m = 1, \dots, N_{i,p}, \\ n = 1, \dots, N_{j,p} \end{array} \right\} \quad (5)$$

Similar to CP_{τ} , to compute $CP_{\tau_{min}}$ and $CP_{\tau_{max}}$ we take the mean over all the P clusters which contain events from electrodes i and j ,

$$CP_{\tau_{min}} = \frac{1}{P'} \sum_{p=1}^{P'} CP_{\tau_{min}^p} \quad (6)$$

$$CP_{\tau_{max}} = \frac{1}{P'} \sum_{p=1}^{P'} CP_{\tau_{max}^p} \quad (7)$$

To compute the connection frequency we first define the measure CP_{λ^p} between two electrodes in a cluster p based on the possible number of connections as,

$$CP_{\lambda^p} = N_{i,p}N_{j,p} \quad (8)$$

where $N_{i,p}$ and $N_{j,p}$ are the total number of events detected on channels i and j in cluster p . Here, $CP_{\lambda_{ij}^p}$ represents the possible connections between all events on electrodes i and j in cluster p . If within a given cluster p , events from electrodes i and j do not co-occur, then we set $CP_{\lambda_{ij}^p} = 0$

If there are a total of P clusters, the number of connections between electrodes i and j is given by the CP metric,

$$CP_{\lambda} = \frac{1}{N_i N_j} \sum_{p=1}^P CP_{\lambda^p} \quad (9)$$

where N_i and N_j are the total number of events detected on channels i and j . The term $N_i N_j$ in the denominator normalizes CP_{λ} to values in the range of 0 and 1.

Simulations

In order to test the proposed CP-based metrics, we used a network of three neural mass models to simulate EEG data ($T = 15$ seconds). Figure 2 (a) shows the simulated model where source x_1 and x_2 interact with a delay of 3 seconds, while x_3 is non-interacting. The ordinary differential equations describing each source using a neural mass model²⁷ are provided in the Supplementary material, and the parameters are set as given in²⁷. To investigate the effect of noise and the threshold for event detection on the performance of the CP-based metrics we set SNR to 0.5, 1, 2 and 3 while the event-detection thresholds were set to $\pm 1.5\bar{\sigma}$, $\pm 2\bar{\sigma}$, $\pm 2.5\bar{\sigma}$ and $\pm 3\bar{\sigma}$. The simulated signals at various SNR are shown in Figure 2 (b)

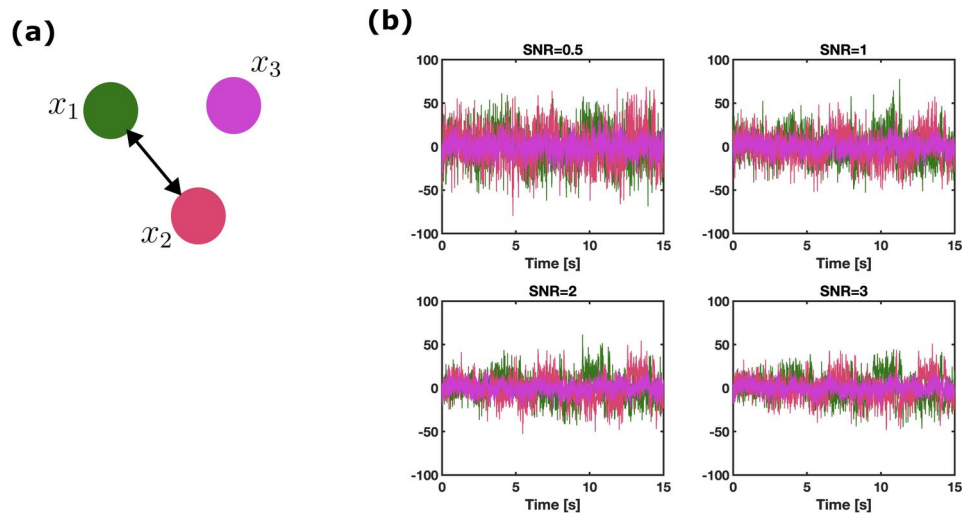


Fig. 2. Simulation of EEG signals using neural mass models. **(a)** Interaction structure between the signals. **(b)** Simulated EEG signals using three neural mass models at various SNR.

Computation of other functional connectivity metrics

For the same EEG records, we computed the commonly used spectral-based functional connectivity metrics of phase locking value, absolute and imaginary coherence as well as mutual information. The spectral-based connectivity matrices were extracted for δ (0.5 to 4 Hz), θ (4 to 8 Hz), α (8 to 13 Hz) and β (13 to 30 Hz) bands.

Spectral-based measures

The cross-spectral density matrix was computed from the EEG signals to estimate the absolute and imaginary part of coherence. The coherence measure $C(f)$ between two EEG signals from electrodes i and j was calculated as,

$$C(f) = \frac{S(f)}{\sqrt{(S_i(f)S_j(f))}}, \quad (10)$$

where the cross-spectral density $S(f)$ describes the cross-correlation between a pair of electrodes (zero-mean and unit variance) in the frequency domain (at frequency f), while $S_i(f)$ and $S_j(f)$ refer to the individual power spectra for signals from electrode i and j . Based on $C(f)$, absolute coherence (*absCoh*) and imaginary part of coherence (*imCoh*)¹³ are defined as $|C(f)|$ and $\Im\{C(f)\}$ respectively.

The PLV between two EEG signals from electrodes i and j was calculated as,

$$PLV \triangleq \left| T^{-1} \sum_{t=1}^T e^{i\Delta\phi(t)} \right| \quad (11)$$

where $\Delta\phi(t) = \phi_i(t) - \phi_j(t)$, and $\phi_i(t), \phi_j(t)$ are the instantaneous phase angles obtained using the analytical signal² and T is the number of time samples. To obtain the analytical signal, we convolved the EEG signals with Morlet wavelets²⁸.

Mutual information

The amount of information one random variable X provides about another random variable Y can be quantified using the information-theoretic measure MI or mutual information. Given two discrete random variables, MI is computed as

$$MI = \sum_{x \in X} \sum_{y \in Y} p(x, y) \log \left(\frac{p(x, y)}{p(x)p(y)} \right) \quad (12)$$

where $p(x, y)$ is the joint probability density function (PDF) of X and Y , and $p(x)$ and $p(y)$ are the marginal PDFs. If two random variables are independent, then the mutual information is zero. In general, the strength of interaction between two random variables is defined by the value of MI. In this case, the two random variables represent the EEG signals from two electrodes. In this work we used the Kraskov-Stögbauer-Grassberger (KSG) estimator approach to calculate MI as the KSG estimator performed the best in distinguishing between EEG tasks in this study compared to other estimators of MI.

Statistical analysis

We conducted statistical analysis in three different ways, which we refer to as *TEST 1*, *TEST 2* and *TEST 3* in the article to assess the ability of the newly proposed connectivity measures based on coherence potentials to distinguish between different tasks, and to compare them with other functional connectivity metrics (absCoh, imCoh, PLV and MI). We define K_i^A and K_i^B as the upper triangle of a symmetric connectivity matrix for subject i for tasks A and B, computed using CPs or other connectivity methods used in this study. We performed permutation testing using the three approaches described below and in all cases we corrected for multiple comparisons using the Bonferroni-Holm method.

TEST 1: Group-level analysis

We computed the mean of the pairwise connectivity values, which in our case amounts to 91 pairwise connectivity values, (considering the upper triangle of symmetric 14×14 connectivity matrix and excluding the diagonals) across each the subjects ($N = 25$) for each task. In Figure 3 this is denoted as \bar{K}^A and \bar{K}^B for any two tasks A and B. To test the null hypothesis that the functional connectivity matrices are not different between the two tasks, permutation testing was conducted to generate the null distribution using 5000 permutations. The difference in distance between the cumulative distribution functions (CDFs) of the pairwise connectivity values for the two tasks was used as the test statistic in permutation testing for comparing task pairs.

TEST 2: Group-level analysis

For this group-level analysis, we computed the mean of pairwise connectivity values (= 91) for each subject and task. For any two tasks A and B, this results in two vectors $\bar{k}^A = [\bar{k}_1^A \ \bar{k}_2^A \ \dots \ \bar{k}_{25}^A]^\top$ and $\bar{k}^B = [\bar{k}_1^B \ \bar{k}_2^B \ \dots \ \bar{k}_{25}^B]^\top$ as shown in Figure 3. Again, to test the null hypothesis that the functional connectivity matrices for the two tasks A and B are not different, permutations testing was conducted using 5000 permutations. The difference in means of \bar{k}^A and \bar{k}^B was used as the test statistic for permutation testing.

TEST 3: Subject-level analysis

In subject-level analysis, the null hypothesis that the difference between pairwise connectivity values $K_i^A \in \mathbb{R}^{91 \times 1}$ and $K_i^B \in \mathbb{R}^{91 \times 1}$ for an individual subject i is not different between any two tasks A and B. Permutation testing with 5000 permutations was used to test for significance in connectivity matrices between two tasks for each subject. The percentage of subjects that reject the null hypothesis is then reported.

Results

Coherence potentials follow a power law distribution in EEG

Coherence potentials are events with similarly shaped waveforms that occur across multiple electrodes and are identified here by clustering based on a correlation based distance metric that compares the shape of the waveform of each pair of events. The choice of a distance threshold is thus an important parameter in the definition of coherence potentials.

To see how clusters changed with the threshold of this distance metric we first looked at the relationship between the number of clusters and cluster size (i.e., number of events in a cluster) for different cluster thresholds. For all the tasks, pooled across all the subjects, the resulting cluster size distribution could be well fit by a power-law distribution for cluster thresholds 0.1, 0.3 and 0.5, with the number of clusters decreasing

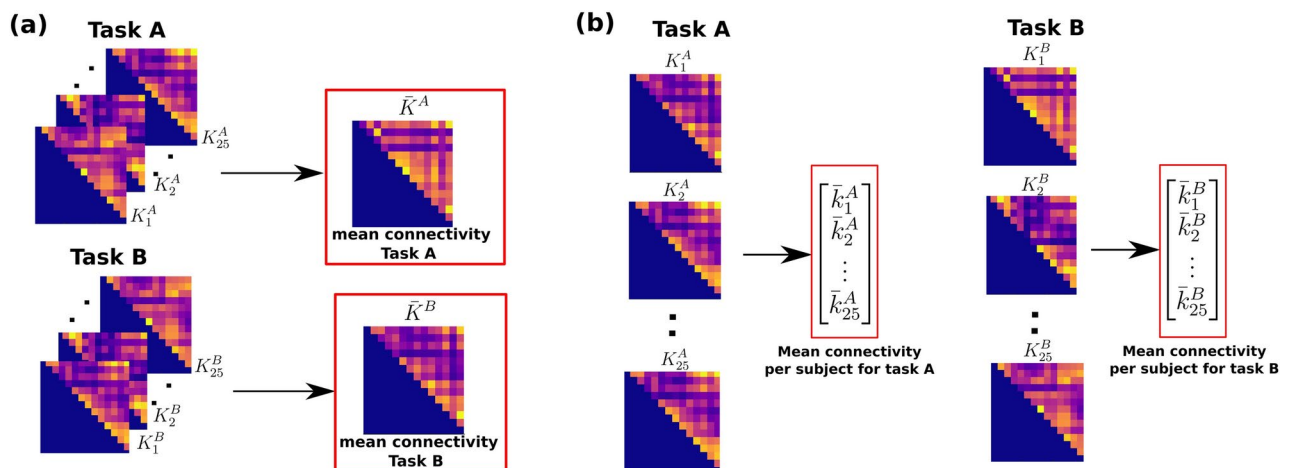


Fig. 3. Statistical testing approaches to analyze group-level difference between a pair of tasks. **(a) TEST 1** - Mean pairwise connectivity values across 25 subjects is computed for each task (shown in red box) and a permutation test is used to assess the difference between the two tasks. **(b) TEST 2** - Pairwise connectivity values are averaged to obtain a single connectivity value per subject for each task (shown in red box). Permutation testing is used to assess the difference between two tasks.

linearly with larger event clusters on a logarithmic scale (Figure 4 (a) - (d) for tasks EC, EO, PC and WM). The slope of the distribution was steeper as the cluster threshold decreased with a power-law exponent α , averaged across EC, EO, PC and WM, of -2.32 ± 0.07 , -1.49 ± 0.09 and -1.27 ± 0.12 for cluster thresholds 0.1, 0.3 and 0.5 respectively with goodness of fit ranging between 0.95 and 0.99). The power law distribution suggests scale free behavior and the exponent of ≈ 1.5 at cluster threshold 0.3 aligns with the avalanche statistics of coherence potentials identified in both rats and monkeys^{21,22}, and is associated with the concept of criticality^{29,30}. We thus used 0.3 as the threshold going forward where coherence potentials are defined as clusters arising at this threshold of similarity of waveform shape.

We note that for the higher clustering threshold of 0.8 (corresponding to a lower threshold of similarity), the majority of events ($\approx 95\%$) were within a single cluster and thus the behaviour was not explained well by the power-law fit (the goodness of fit for power-law fit ranged between 0.4 - 0.6 with exponent -0.1 ± 0.08).

The relationship between the number of events in a cluster and the number of clusters did not change qualitatively when analyzed for different event detection thresholds - $\pm 1\sigma$, $\pm 2\sigma$, $\pm 3\sigma$ and $\pm 4\sigma$. Supplementary Figure S1 shows that for a given clustering threshold ($= 0.3$), as the event detection threshold increases, the number of clusters decrease as expected, but the relation between cluster size and number of cluster continues to follow a power-law distribution.

From the simulation results (See supplementary figures S7-S10) we can see that at event detection threshold of $\pm 1.5\sigma$, in addition to the true interaction between x_1 and x_2 , connectivity between x_3 , other sources are detected as well. However for thresholds $\geq \pm 2\sigma$ the correct interaction structure is recovered with the average inter-event interval CP_τ approaching 3 seconds (ground truth) as the signal to noise ratio (SNR) increases. Similar results were obtained from other CP-based connectivity metrics - $CP_{\tau_{max}}$, $CP_{\tau_{min}}$ and CP_λ where we observed the recovery of true interaction structure from thresholds $\geq \pm 2\sigma$.

Coherence potential characteristics differ across tasks

For coherence potentials to carry information their characteristics must vary across tasks. Here we show that the cluster size distribution varied significantly across tasks in the tails. Altogether clusters with large event sizes of 50 or more were most dominant across subjects when performing the PC task while few subjects had such large events when performing the WM task (Figure 5 (a)). EC and EO were in between, with EO more similar to the PC task. Given that these recordings are carried out with 14 channel EEG devices, this indicates that the same waveform shape recurs many more times on the same sets of electrodes over the course of the PC task compared to the WM task.

In addition to the event size, for each pair of electrodes i and j we looked at the inter-event interval CP_τ , and averaged across all pairs of electrodes for each subject which is referred to as \overline{CP}_τ . Overall the inter-event intervals were significantly shorter when subjects were performing the WM task compared to all other tasks and longest when performing the PC task. Figure 5 (b) shows that the WM task has a higher percentage of subjects

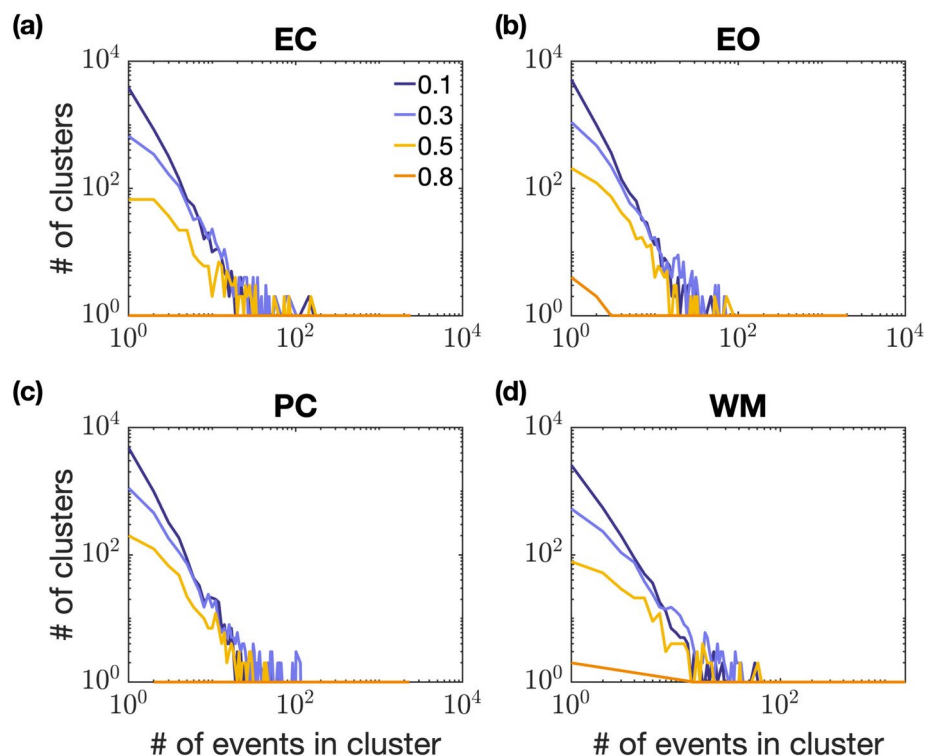


Fig. 4. Cluster size distributions for tasks EC, EO, PC and WM (a-d) at various clustering thresholds showing the relation between number of events in cluster (i.e. cluster size) and the number of clusters.

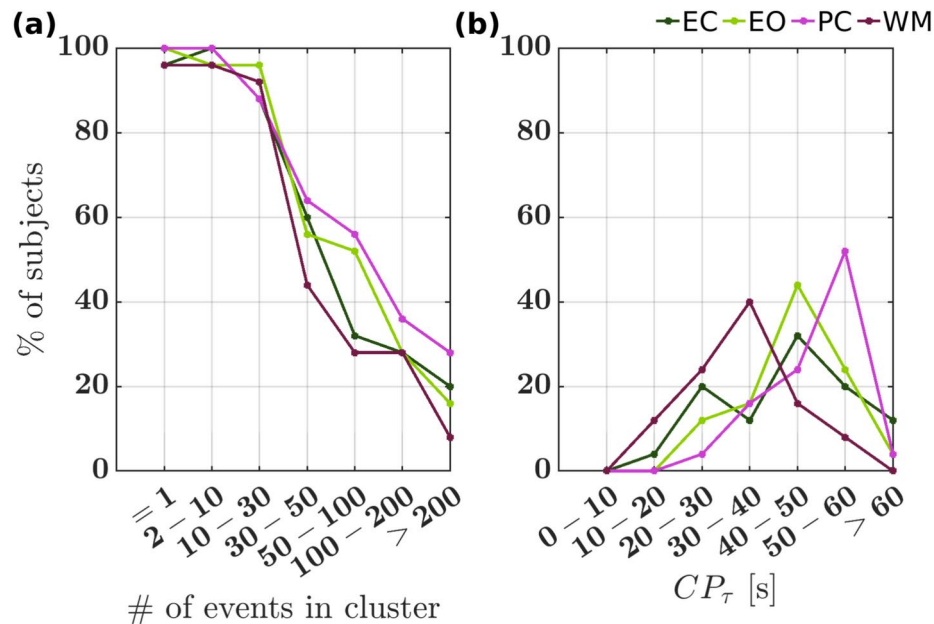


Fig. 5. Number of subjects with different event sizes (a) and inter-event interval (b) for EC, EO, PC and WM tasks. Here CP_τ here refers to the mean of $CP_{\tau_{ij}}$ (See Equation 3) across all electrode pairs for each subject.

with a mean τ between 10 and 40 s while mean \overline{CP}_τ in the range of 50–60 seconds was most prominent for PC followed by the EO task.

Coherence potential based connectivity measures distinguish more robustly between tasks across statistical tests

Group-level analysis: TEST 1

Figure 6 (a–d) shows the cumulative distribution function (CDF) of pairwise CP connectivity measures - CP_τ , $CP_{\tau_{max}}$, $CP_{\tau_{min}}$ and CP_λ , averaged across 25 subjects as described in Section 2.6 and Figure 3(a). The results presented here use the threshold of $\pm 2\sigma$ for event detection. However, varying the threshold from $\pm 1\sigma$ to $\pm 4\sigma$ could still distinguish between the tasks demonstrating its robustness with respect to this thresholding parameter. The results for CP-based metrics for various thresholds tested are shown in Supplementary Figures S2–S5.

For the WM task, electrode pairs occurring within clusters or coherence potentials had lower (CP_τ ranging between 20 and 30 seconds, with mean 31.4 ± 4.8 seconds), whereas for the PC task the electrode pairs have longer CP_τ (ranging between 40 and 60 seconds, with mean 48.8 ± 5.5 seconds) as shown in Figure 6 (a). The CP_τ values for EC (mean - 42.4 ± 4.1 seconds) and EO (mean 44.8 ± 4.3 seconds) tasks were distributed between the WM and PC tasks.

We similarly calculated CP_λ defined as the number of times they co-occurred within a cluster or coherence potential, for each pair of electrodes and plotted its CDF (See Figure 6 (b)). For the WM task, pairs of electrodes had much higher $CP_{\lambda_{ij}}$ (mean 0.26 ± 0.04) compared to other tasks followed by EC (mean 0.22 ± 0.03), PC (mean 0.16 ± 0.04) and EO (mean 0.14 ± 0.04) tasks. For the PC task, the CDF of CP_λ was similar to the EO task but with higher values. In case of both CP_τ and CP_λ , the difference between the CDFs of EC, EO, PC and WM was statistically significant based on two-sample permutation testing of the difference in Kolmogorov-Smirnov statistic between the CDFs with multiple comparisons corrected using the Bonferroni-Holm method.

In the case of $CP_{\tau_{max}}$ (Figure 6(b)), except for the difference between EC (mean 79.9 ± 6.8 seconds) and EO (mean 79.7 ± 6.4 seconds), and in the case of $CP_{\tau_{min}}$ (Figure 6(c)) except for the difference between EO (mean 17.4 ± 4.3 seconds) and PC (mean 17.9 ± 4.7 seconds), statistically significant differences were found between the CDFs for all other task pairs. Similar to CP_τ , we observed WM task had lower $CP_{\tau_{ij,max}}$ (mean 58.9 ± 7.8 seconds) and $CP_{\tau_{ij,min}}$ (mean 10.4 ± 3.4 seconds) compared to other tasks, while for the PC task higher values were observed ($CP_{\tau_{max}}$ with mean 89.5 ± 9.02 seconds and $CP_{\tau_{min}}$ with mean 17.9 ± 4.7 seconds).

In Figure 7 we show a spatial visualization of the coherence potential characteristics (averaged over 25 subjects for each of the tasks - EC, EO, PC and WM). Here the line thickness between electrodes represents the connection frequency CP_λ while the color represents the inter-event interval CP_τ between the electrodes i and j , both averaged across subjects. This visualization shows a clear global increase in connection frequency in the EC task versus EO. It also shows that the WM task is characterized by higher connection frequencies and lower inter-event intervals (indicating faster speed) across all electrode pairs compared to all other tasks. In contrast the PC task is characterized by higher inter-event intervals (indicating slower speeds) particularly in contrast to the WM, and high connection frequencies only at select pairs of electrodes. Altogether this shows that each task is associated with distinct global spatiotemporal characteristics of coherence potentials.

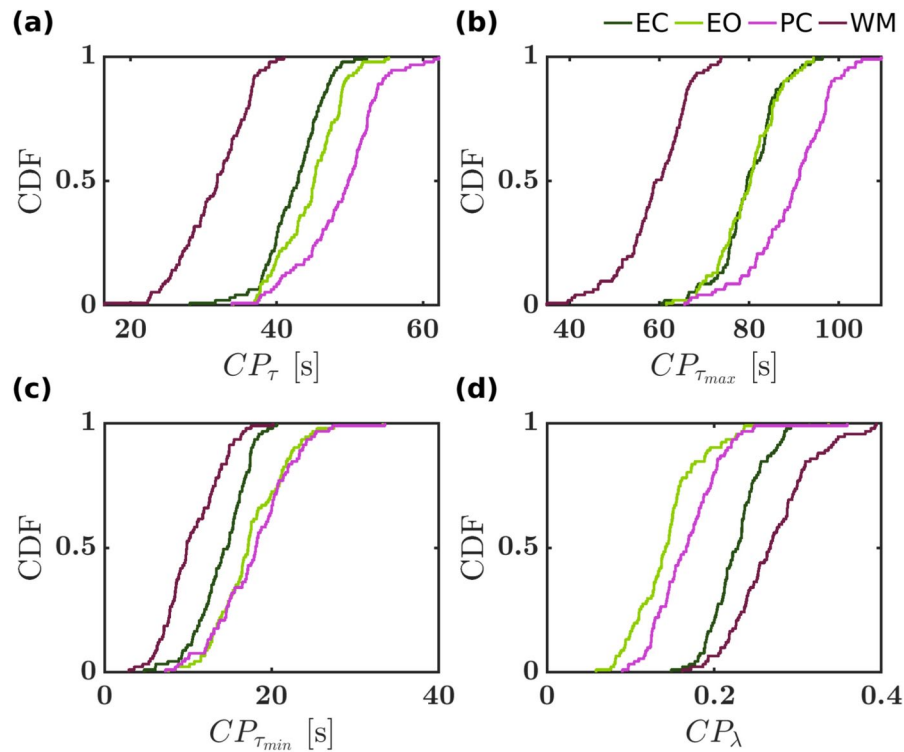


Fig. 6. CDF plots for group level comparison with TEST 1 for all the tasks - EC, EO, PC and WM. (a–d) The CDFs are plotted by averaging the CP connectivity measures over all subjects for each electrode pair and the distribution is plotted over all the electrode pairs (91 pairs as there are 14 electrodes and the CP connectivity measures are symmetric).

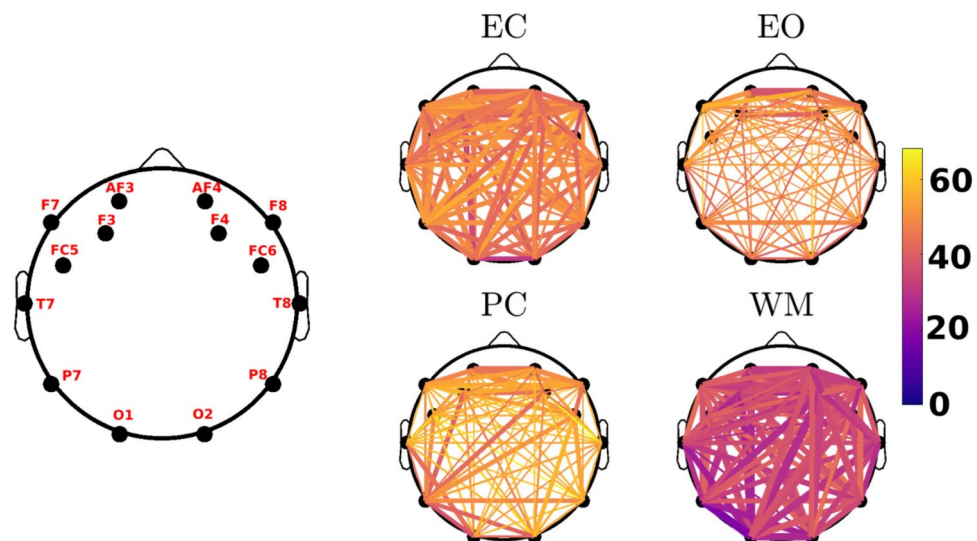


Fig. 7. Network plot with electrodes as the nodes and edge color represented by inter-event interval (CP_{τ}) and thickness by connection frequency (CP_{λ}). Both these are averaged over 25 subjects in the network plot (See TEST 1). The colorbar represents CP_{τ} in seconds.

We next looked at how various other methods of estimating functional connectivity were able to distinguish between the different tasks using group-level analysis TEST 1. As in the case of CP metrics shown above, we performed permutation testing using the Kolmogorov-Smirnov distance statistic to test for statistical significance between the CDFs of various tasks with multiple comparisons corrected using the Bonferroni-Holm method.

Figure 8 shows the empirical CDF across electrode pairs, averaged over 25 subjects, for *absCoh*, *imCoh*, *PLV* and *MI*. Here the spectral connectivity metrics are shown only for the α band. Figures for results in the other

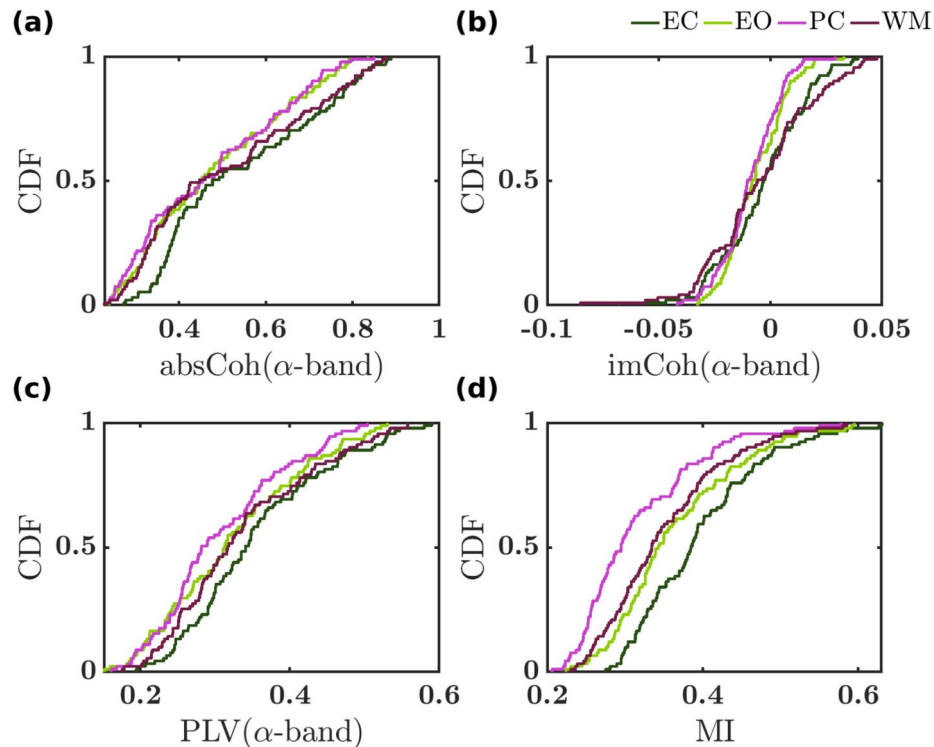


Fig. 8. CDFs of other connectivity measures for group-analysis using *TEST1*. (a) Absolute coherence, (b) Imaginary part of coherence, (c) Phase locking value and (d) Mutual information for all the four conditions - EC, EO, PC and WM. The measures for each pair were averaged across all the subjects and, averages for the CDF over all possible electrode pairs (14 electrode, 91 pairs) are plotted. For the spectral-based connectivity measures (a-c) only results from the α -band are plotted.

frequency bands are shown in Supplementary Figure S6. Among the spectral-based connectivity metrics *absCoh* showed statistically significant differences between the CDFs of EC and EO and EC and PC tasks in the δ , θ and α bands (α band shown in Figure 8 (a)). Phase locking value showed statistically significant differences between the CDFs of EC and PC tasks in the θ , α and β bands (Figure 8 (c)). The CDFs between EO and PC, and EO and WM, and EC and WM were not found to be statistically significant after correcting for multiple comparisons for any of the spectral connectivity metrics, in any of the frequency bands. In case of mutual information (see Figure 8 (d)), statistically significant differences were found between the CDFs of all task pairs except between the EO and WM tasks.

All the *p*-values obtained from permutation tests comparing the tasks using group-level analysis *TEST 1* are reported in Supplementary Table S1 for the CP connectivity measures and other connectivity measures used in this work.

Group-level analysis: *TEST 2*

Next, we quantified the statistical significance between each pair of tasks at group-level by computing the mean of pairwise functional connectivity metrics for each subject as described in Section 2.6 and illustrated in Fig. 3. Table 1 shows the *p*-values obtained via permutation testing of the difference in means between each pair of tasks for 25 subjects using CP connectivity measures and other connectivity measures. Significant *p*-values, after correcting for multiple comparisons with the Bonferroni-Holm method are in bold. In case of spectral-based connectivity measures, we show the results only in the α band. We can see that among the CP connectivity measures \overline{CP}_τ (i.e., mean of CP_τ across all channel pairs) distinguishes between EO and WM and PC and WM, while $\overline{CP}_{\tau_{max}}$ distinguishes between EC and WM, EO and WM and PC and WM, and $\overline{CP}_{\tau_{min}}$ distinguishes between PC and WM. The CP connectivity measure \overline{CP}_λ does not distinguish between any tasks at a group level. Furthermore, CP-based measures also failed to distinguish between EC and EO, and EC and PC, and EO and PC after correcting for multiple comparisons.

In contrast, both the spectral-based connectivity measures - \overline{absCoh} , \overline{imCoh} and \overline{PLV} , and \overline{MI} , which are the means of the pairwise connectivity values for each subject, were not able to distinguish between any task pairs at group level using *TEST 2*. In case of spectral-based methods, statistically significant differences were not found in any of the frequency bands tested. Thus, only results for the α band are reported here.

Overall, our results demonstrate that only CP connectivity measures are collectively able to distinguish between certain task pairs (PC and WM, EO and WM and EC and WM) at a group level when mean pairwise connectivity values are used as statistic to discriminate between the tasks.

	EC-EO	EC-PC	EC-WM	EO-PC	EO-WM	PC-WM
\overline{CP}_τ	0.51	0.04	0.01	0.02	0.002	3e-5
$\overline{CP}_{\tau_{min}}$	0.25	0.02	0.21	0.42	0.02	0.006
$\overline{CP}_{\tau_{max}}$	0.41	0.37	0.01	0.03	1.2e-4	1.34e-5
\overline{CP}_λ	0.04	0.33	0.39	0.43	0.02	0.2
$\overline{PLV}(\alpha\text{-band})$	0.44	0.23	0.63	0.70	0.75	0.47
$\overline{absCoh}(\alpha\text{-band})$	0.10	0.10	0.21	0.86	0.45	0.37
$\overline{imCoh}(\alpha\text{-band})$	0.27	0.054	0.75	0.38	0.46	0.11
\overline{MI}	0.73	0.29	0.57	0.55	0.87	0.61

Table 1. Results from group-level analysis using *TEST 2* for the connectivity measures. For each subject a mean of the pairwise connectivity values was obtained for each task. The *p*-values were then obtained using a permutation test comparing two different tasks across all the subjects. Significant *p*-values obtained after correcting for multiple comparisons using the Bonferroni-Holm method are in bold.

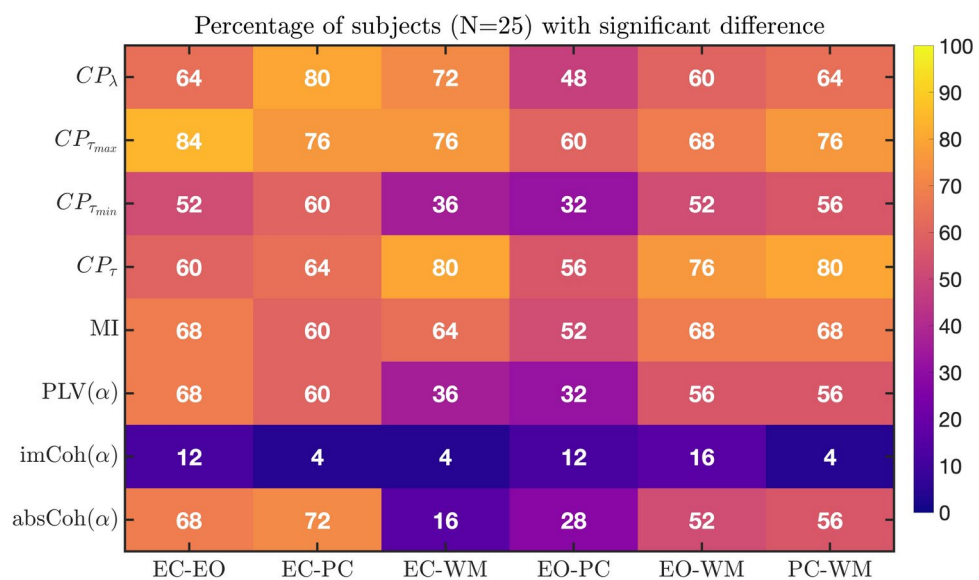


Fig. 9. Comparison of subject-level permutation test results for the proposed CP connectivity measures with spectral-based connectivity metrics (α -band) and mutual information using *TEST 3*. The color corresponds to the percentage of subjects with significant difference after correcting for multiple comparisons using the Bonferroni-Holm method.

Subject-level analysis: *TEST 3*

Our results from the subject-level analysis (*TEST 3*) depicted in Figure 9 show that CP based connectivity measures perform better in the aggregate across all task pairs with the most robust results between WM and both the EC and PC tasks (EC-WM : 80% and 76% for CP_τ and $CP_{\tau_{max}}$ respectively, and PC-WM : 80% of the subjects for CP_τ) while all other connectivity measures performed substantially worse. We also observe that *absCoh* performed the best among the other connectivity measures, comparable to CP measures $CP_{\tau_{max}}$ and CP_τ in distinguishing between EC and PC tasks (72% for *absCoh* vs 76% for $CP_{\tau_{max}}$ and 80% for CP_λ). All the connectivity metrics performed worst in distinguishing between EO and PC with *MI* performing almost as well as CP measures (52% for *MI* vs 60% for $CP_{\tau_{max}}$). Overall *imCoh* performed the worst among the connectivity measures with no case above 16%. For the spectral-based measures only results from the α band is shown as the α band outperformed other bands for the majority of task pairs. The exceptions were the θ and δ bands for *imCoh* and *absCoh* for EC-WM task comparisons. Results from other frequency bands are compiled and shown in Supplementary Table S2.

Discussion

In this work, we have described a new method for estimating functional connectivity from EEG that utilizes the concept of coherence potentials or CPs, which are defined as large amplitude deflections (relative to baseline) that are clustered based on similarity of waveform shape. We derived the following novel connectivity metrics based on CP : 1) inter-event interval between the peaks of waveforms occurring on each electrode pair CP_τ

, $CP_{\tau_{max}}$ and $CP_{\tau_{min}}$ that describes the temporal aspect of connectivity and 2) frequency of co-occurrence of electrode pairs, normalized between 0 and 1, within CP, CP_{λ} that describe the spatial aspect of connectivity.

We demonstrate that our proposed metrics differ significantly between each of four task conditions - EO, EC, PC and WM, and perform consistently better than other commonly used functional connectivity metrics of *absCoh*, *imCoh*, *PLV* and *MI* in distinguishing between task conditions when tested using both group-level and subject-level analysis.

Altogether these metrics provide a novel perspective on the nature of connectivity in the brain. Based on clusters of similar waveforms, they suggest the binding of regions with distinct structurally complex patterns of activity with spatiotemporal characteristics that are task dependent.

Coherence potentials in the EEG

The phenomenon of CPs has been observed using local field potentials in *in vitro* organotypic slice cultures²¹, cortex of awake monkeys²¹ recorded using microelectrode arrays, and electrocorticography recordings in humans performing a visuomotor task²². It has been previously demonstrated that CPs propagate without distortion at other cortex sites with timescales in the range of tens of milliseconds for microelectrode arrays²¹ and hundreds of milliseconds for electrocorticography recordings²². Furthermore, the size distribution of CPs mirrors the power-law distribution²¹ of neuronal avalanches^{25,29}.

Despite having a much lower spatial resolution and more pronounced volume conduction effects compared to microelectrode arrays and ECoG recordings, we observed spatiotemporal patterns of coherence potentials in EEG recordings as well. However, the timescale within the CPs (measured in terms of inter-event intervals across clusters) ranged from a few seconds to approximately 60 seconds across the tasks. One possible explanation for these longer timescales is that only the largest and longest-lasting cascades of CPs appeared at other EEG electrode sites without distortion due to volume conduction.

We observed a power-law like relation between the size of clusters and number of clusters, which have been previously observed for coherence potentials in human ECoG recordings²². Specifically for cluster threshold 0.3, the exponent was ≈ -1.5 which is characteristic of neuronal networks operating at criticality^{31–33}, optimizing for information processing in neuronal networks³⁴. We therefore use a clustering threshold of 0.3 for all the analysis. However, despite a broadly power-law like behaviour for the cluster size distribution, there were key differences in the tail for all the tasks, with the WM task characterized by fewer large clusters of 30 or more events (i.e. large coherence potentials) compared to other tasks, while the PC task had many more large clusters in the range of 50 to 100 events per cluster for $\approx 60\%$ of the subjects (Figure 5 (a)).

Comparison of coherence potential metrics to other metrics of functional connectivity

While testing for significant differences between tasks using different levels of statistical testing - 1) a group-level test averaged across subjects (*TEST 1*), 2) a group-level test with one mean connectivity value per subject (*TEST 2*) and 3) a subject-level test comparing between tasks per subject using pairwise connectivity values (*TEST 3*), we found that CP-based connectivity metrics were consistently able to distinguish between different tasks compared to other functional connectivity metrics.

CP-based metrics outperform other functional connectivity metrics using group-level *TEST 1*, effectively distinguishing between all task pairs. Only *MI* gave results comparable to CP connectivity measures, failing to distinguish only between EO and WM tasks. However it is to be noted here that results from *MI* depended on the methods used to estimate it. The results presented here are from KSG-based estimation of *MI*, while k-nearest neighbor-based implementation of *MI* could not distinguish between any of the tasks.

While the CP connectivity measures distinguished robustly between task conditions compared to other metrics, they were directionally similar and consistent with results from other metrics shown here. The proposed CP connectivity measure CP_{λ} was significantly higher in EC task compared to EO, as were *MI*, *absCoh* and *PLV* when analyzed at the group-level by averaging across the subjects (*TEST 1*). These results are also consistent with previous EEG studies which have shown increased connectivity during EC compared to EO using nonlinear measures such as synchronization likelihood¹², transfer entropy³⁵ and multivariate transfer entropy³⁶, particularly in the α band, which is also referred to as α desynchronization. This was also demonstrated using intracranial EEG with *PLV* and phase lag index as connectivity measures in³⁷. Also, using functional MRI, Han and colleagues³⁸ showed that there is increased connectivity during EC compared to EO task. Furthermore, several studies using resting state data from the human connectome project have been studied with fMRI and MEG^{39–42} and have demonstrated the existence of spontaneous functional connectivity among distributed brain regions⁴³. Thus, the characterization of synchronization strength between EEG signals by CP_{λ} is consistent with other functional connectivity metrics reported above.

Similarly, CP-based measures show both increased connection frequency CP_{λ} and lower inter-event interval CP_{τ} in WM compared to the tasks EC and EO at group level (*TEST 1*), which is consistent with previous studies using other functional connectivity metrics. These include EEG studies which have shown increased synchronization levels in a visual WM task using synchronization entropy compared to resting EC⁴⁴, and in a different WM task (delayed response visual and visuo-spatial task) using *absCoh* compared to resting EO in humans⁴⁵. In⁴⁶, increased synchronization was also observed during a WM task (delayed matching-to-sample task) using intracranial EEG in monkeys using the measure *PLV* compared to eyes open task. However, in our work we observed group-level difference (*TEST 1*) between WM and EC using *absCoh*, *PLV* in the δ , θ and α bands and *MI*, but we did not observe any group-level difference between EO and WM task using these metrics. Since EC condition has a strong oscillatory component, we hypothesize that it was easier for other functional connectivity metrics to distinguish between EC and other tasks. Furthermore different experimental design of WM task could have contributed to the differences between WM and EO in^{45,46}. This further demonstrates that CP connectivity measures can robustly distinguish between tasks that do not differ only due to strong oscillatory

component and also using only one trial. Following a similar trend, when we did the subject-level analysis, again the spectral-based measures generally showed good performance in distinguishing between EC and other conditions, while the performance became relatively worse when distinguishing between EO condition and PC or WM tasks and between PC and WM tasks. Interestingly only *MI* gave close to a comparable performance to CP-based metric at group-level using *TEST 1* and at subject-level (*TEST 3*) only giving poor performance for EO vs WM. We hypothesize the reason for such comparable performance between these two methods could be due to no inherent assumptions about the nature of interaction (linear or non-linear) unlike spectral-based measures that assume linear interaction.

When tested at group-level by collapsing the pairwise connectivity values to a single number using the mean value (*TEST 2*), none of the other connectivity metrics could distinguish between the tasks, whereas three CP-based metrics - CP_{τ} , $CP_{\tau_{max}}$ and $CP_{\tau_{min}}$ could collectively distinguish between EC-WM, EO-WM and PC-WM tasks. The results from both the group-level analyses imply that these CP-based metrics can capture certain aspects of connectivity difference between cognitive tasks that are not limited by the number of trials and does not require *a priori* hypothesis on the specific frequency bands where interaction of relevance might happen. Furthermore, CP-based metrics are also able to distinguish between certain cognitive tasks when the pairwise connectivity values are collapsed into a single number (e.g., mean) which other functional connectivity metrics failed to do. This implies that CP-metrics are able to better characterize certain global aspects of connectivity networks (such as mean value) which are task dependent. However none of the CP-based metrics or other connectivity metrics could distinguish between EC-EO, EC-PC and EO-PC when the connectivity values were collapsed to a single number. This indicates that distinguishing between these tasks require more information from all the electrodes, which we observed in the results from (*TEST 1*) where CP-based metrics again outperformed other connectivity metrics when all pairwise connectivity values were considered.

We also note that among the spectral-based connectivity methods we tested, *imCoh* generally showed poor performance at both the group level and subject level in distinguishing between tasks. Some possible reasons are that although *imCoh* has been demonstrated to avoid spurious connectivity due to volume conduction by neglecting the real part, this also effectively ignores true connectivity that occur at 0 or π radians⁴⁷. Furthermore, in⁴⁸ it was shown that the imaginary part of coherence can be affected by volume conduction and noise due to the way it is normalized.

Overall, these results imply that CP-based connectivity metrics capture spatio-temporal fingerprints in EEG signals which vary under different task conditions and may not have a specific frequency of interaction.

Insights into brain connectivity based on CP differences between tasks

Differences in CP metrics between tasks that are of greater magnitude and statistical significance compared to traditional metrics suggests that not all activity is equal and that these embedded structures (i.e. CPs) are more informative of task activity or brain state. As CPs are based on similarity of complex waveform shapes, these results also suggest a specific binding of regions with distinct structurally complex patterns of activity rather than simply at specific frequencies. In addition, differences in the spatial and temporal characteristics of CPs as captured by the metrics of connection frequency (CP_{λ}) and inter-event intervals or timescales (CP_{τ}) between tasks, indicate that the spatiotemporal characteristics of binding has significance for the nature of task the brain is engaged in.

For example, these results provide several novel insights into connectivity differences between resting state (EC and EO) vs PC and between PC and WM task, that have not been hitherto investigated. WM is characterized by globally faster and stronger connection frequency compared to all other tasks (i.e. across all channel pairs; See Figure 5 and 6 (a-b)), which imply overall greater synchronization and shorter time-scales within CPs in the WM task compared to other tasks. In contrast, the PC task is characterized by high inter-event intervals with $\approx 60\%$ of subjects having mean-IEI between 50 and 60 seconds compared to other tasks (See Figure 5 and 6(a-b)). Furthermore, PC had more variability in connection frequency across channel pairs. Among the other tasks EO had the weakest connection frequency and EC the strongest. Altogether, the differences among tasks appear to be global with greater regional specificity in the PC task alone. A possible interpretation of this is that the WM task requires faster but weaker global cooperation while the PC task involves more regional specificity with stronger cooperation such that events within coherence potentials may repeat more often on the same electrode.

Altogether understanding the spatiotemporal structure of CPs isolated from the rest of the activity provides greater information and separability relative to standard measures that utilize the full EEG signal with alternative approaches.

Volume conduction

In our study we have estimated functional connectivity directly from EEG recordings. Due to the issue of volume conduction⁴⁹, several studies have emphasized the importance of estimating functional connectivity in source space^{10,12} i.e. estimating functional connectivity between the source signals estimated from EEG recordings⁵⁰ instead of estimating it directly from the EEG recordings. Thus, we note that interpreting connectivity results based on sensor-level analysis requires caution as signal mixing due to volume conduction can affect the results. However as noted in³, estimated source activities are not necessarily independent, with volume conduction effects still present in them. Furthermore, source estimation involves the complex step of constructing forward models, which may not be realistic or accurate in terms of tissue anisotropy or conductivity values and may thus bias the connectivity results⁵¹.

In situations where speed and cost of EEG recordings are key considerations, obtaining functional connectivity estimates directly from EEG recordings could be the only feasible option. In our case the low number of EEG electrodes and the unavailability of MR images for the construction of forward models limits the use of source estimation techniques. Also since we are comparing the functional connectivity measures across

different experimental tasks, any difference obtained between them cannot be explained by volume conduction effects as they should impact the functional connectivity measures similarly across all tasks. Nonetheless, the generality of our proposed approach using coherence potentials would allow estimation connectivity in the source space as well. Combined with accurate forward models and an orthogonalization approach to limit the leakage between source signals⁵², coherence potential based connectivity estimation in source-space can provide valuable insights. Finally, although we used only EEG data in this work, it should be straightforward to apply the proposed algorithm to MEG data as well.

Potential applications of the novel metrics

As demonstrated in this work, given the ability of the proposed coherence potential based metrics to characterize underlying functional connectivity during different task conditions, a straightforward application of our method could be in the early detection of neurological disorders that affect various cognitive tasks. Deficits in working memory have been implicated in mild cognitive impairment, Alzheimer's and Parkinson's disease^{53,54}. In general, any application that requires discrimination between brain states can be explored with our approach. For example, detection in changes in brain state as reflected in functional connectivity during anesthesia or pathological states such as epileptic seizures could be potential applications.

Our results also show interesting shifts in connectivity patterns as cognitive tasks change, for example PC vs WM. Results regarding such shifts could be explored to build new hypotheses on how global brain connectivity changes as tasks shift, which are currently lacking.

Finally, compared to classical connectivity metrics (for e.g. spectral-based methods) our approach is more reliable for computing functional connectivity from scalp-EEG signals. This will increase its utility in clinical applications and naturalistic settings where often only few electrodes are available and thus estimating connectivity in source-space is not possible.

Limitations and future work

We would like to note a few limitations of our study. First, this method cannot be applied to short recordings, for example such as event-related potentials, but rather requires several minutes of recording to obtain sufficient events for the CP-based metrics to extract reliable connectivity from EEG data. Second, at lower event detection thresholds the number of detected events can be very high which can increase the computational cost of the method in constructing the high-dimensional correlation matrix between events. Third, the use of a baseline-to-baseline duration may not be optimal, particularly given the non-stationary nature of EEG. While this work aimed to demonstrate that the concept of coherence potentials can be extended to define a notion of functional connectivity and show that it is able to distinguish between different task-related EEGs, future work will explore constructing CP-based metrics in a temporally dynamic fashion.

Data availability

All the data presented in this study from humans will be made available by the corresponding author on request. An example EEG dataset is made available at <https://gitlab.com/narayanps/sci-rep-coherencepotentials>.

Received: 3 July 2024; Accepted: 11 March 2025

Published online: 28 March 2025

References

1. Friston, K. J. Functional and effective connectivity: A review. *Brain Connectivity*. **1**(1), 13–36 (2011).
2. Bastos, A. M. & Schoffelen, J.-M. A tutorial review of functional connectivity analysis methods and their interpretational pitfalls. *Frontiers in Systems Neuroscience*. **9** (2016).
3. Schoffelen, J.-M. & Gross, J. Source connectivity analysis with MEG and EEG. *Human Brain Mapping*. **30**(6), 1857–1865 (2009).
4. O'Reilly, C., Lewis, J. D. & Elsabbagh, M. Is functional brain connectivity atypical in autism? a systematic review of EEG and MEG studies. *PLoS One*. **12**(5), e0175870 (2017).
5. Du, Y., Fu, Z. & Calhoun, V. D. Classification and prediction of brain disorders using functional connectivity: Promising but challenging. *Frontiers in Neuroscience*. **12**, (2018).
6. Bettus, G. et al. Enhanced EEG functional connectivity in mesial temporal lobe epilepsy. *Epilepsy Research*. **81**(1), 58–68 (2008).
7. Daly, I., Nasuto, S. J. & Warwick, K. Brain computer interface control via functional connectivity dynamics. *Pattern Recognition*. **45**(6), 2123–2136 (2012).
8. Zhang, Y., Yan, G., Chang, W., Huang, W. & Yuan, Y. Eeg-based multi-frequency band functional connectivity analysis and the application of spatio-temporal features in emotion recognition. *Biomedical Signal Processing and Control*. **79**, 104157 (2023).
9. Sakkalis, V. Review of advanced techniques for the estimation of brain connectivity measured with EEG/MEG. *Computers in Biology and Medicine*. **41**(12), 1110–1117 (2011).
10. Gross, J. et al. The neural basis of intermittent motor control in humans. *Proceedings of the National Academy of Sciences*. **99**(4), 2299–2302 (2002).
11. Lachaux, J.-P., Rodriguez, E., Martinerie, J. & Varela, F. J. Measuring phase synchrony in brain signals. *Human Brain Mapping*. **8**(4), 194–208 (1999).
12. Stam, C. J., Nolte, G. & Daffertshofer, A. Phase lag index: Assessment of functional connectivity from multi channel EEG and MEG with diminished bias from common sources. *Human Brain Mapping*. **28**(11), 1178–1193 (2007).
13. Guido N. et al. Identifying true brain interaction from EEG data using the imaginary part of coherency. *Clinical Neurophysiology*. **115**(10), 2292–2307 (2004).
14. Korzeniewska, A., Mańczak, M., Kamiński, M., Blinowska, K. J. & Kasicki, S. Determination of information flow direction among brain structures by a modified directed transfer function (ddtf) method. *Journal of Neuroscience Methods*. **125**(1–2), 195–207 (2003).
15. Zhang, Q. et al. Establishing functional brain networks using a nonlinear partial directed coherence method to predict epileptic seizures. *Journal of Neuroscience Methods*. **329**, 108447 (2020).
16. Baccalá, L. A. & Koichi, S. Partial directed coherence: a new concept in neural structure determination. *Biological Cybernetics*. **84**(6), 463–474 (2001).

17. Liu, L. & Ioannides, A. A. Spatiotemporal dynamics and connectivity pattern differences between centrally and peripherally presented faces. *NeuroImage*. **31**(4), 1726–1740 (2006).
18. Vicente, R., Wibral, M., Lindner, M. & Pipa, G. Transfer entropy—a model-free measure of effective connectivity for the neurosciences. *Journal of Computational Neuroscience*. **30**(1), 45–67 (2010).
19. Subramaniam, N. P., Donner, R. V., Caron, D., Panuccio, G. & Hyttinen, J. Causal coupling inference from multivariate time series based on ordinal partition transition networks. *Nonlinear Dynamics*. **105**(1), 555–578 (2021).
20. Fraser, A. M. & Swinney, H. L. Independent coordinates for strange attractors from mutual information. *Physical Review A*. **33**(2), 1134–1140 (1986).
21. Thiagarajan, T. C., Lebedev, M. A., Nicoletis, M. A. & Plenz, D. Coherence potentials: Loss-less, all-or-none network events in the cortex. *PLoS Biology*. **8**(1), e1000278 (2010).
22. Parameshwaran, D., Crone, N. E. & Thiagarajan, T. C. Coherence potentials encode simple human sensorimotor behavior. *PLoS ONE*. **7**(2), e30514 (2012).
23. Parameshwaran, D., Subramaniam, N. P. & Thiagarajan, T. C. Waveform complexity: A new metric for EEG analysis. *Journal of Neuroscience Methods*. **325**, 108313 (2019).
24. Parameshwaran, D. & Thiagarajan, T. C. High variability periods in the EEG distinguish cognitive brain states. *Brain Sciences*. **13**(11), 1528 (2023).
25. Plenz, D. & Thiagarajan, T. C. The organizing principles of neuronal avalanches: cell assemblies in the cortex?. *Trends in Neurosciences*. **30**(3), 101–110 (2007).
26. Johnson, S. C. Hierarchical clustering schemes. *Psychometrika*. **32**(3), 241–254 (1967).
27. Zavaglia, M., Astolfi, L., Babiloni, F. & Ursino, M. A neural mass model for the simulation of cortical activity estimated from high resolution eeg during cognitive or motor tasks. *Journal of neuroscience methods*. **157**(2), 317–329 (2006).
28. Cohen, M. X. A better way to define and describe morlet wavelets for time-frequency analysis. *NeuroImage*. **199**, 81–86 (2019).
29. Beggs, J. M. & Plenz, D. Neuronal avalanches in neocortical circuits. *The Journal of Neuroscience*. **23**(35), 11167–11177 (2003).
30. Petermann, T. et al. Spontaneous cortical activity in awake monkeys composed of neuronal avalanches. *Proceedings of the National Academy of Sciences*. **106**(37), 15921–15926 (2009).
31. Larremore, D. B., Shew, W. L. & Restrepo, J. G. Predicting criticality and dynamic range in complex networks: Effects of topology. *Physical Review Letters*. **106**(5) (2011).
32. Friedman, N. et al. Universal critical dynamics in high resolution neuronal avalanche data. *Physical Review Letters*. **108**(20), (2012).
33. Shriki, O. et al. Neuronal avalanches in the resting meg of the human brain. *The Journal of Neuroscience*. **33**(16), 7079–7090 (2012).
34. Shew, W. L., Yang, H., Petermann, T., Roy, R. & Plenz, D. Neuronal avalanches imply maximum dynamic range in cortical networks at criticality. *The Journal of Neuroscience*. **29**(49), 15595–15600 (2009).
35. Restrepo, J. F., Mateos, D. M., & López, J. M. D. A transfer entropy-based methodology to analyze information flow under eyes-open and eyes-closed conditions with a clinical perspective. *Biomedical Signal Processing and Control*. **86**, 105181 (2023).
36. Olejarczyk, E., Marzetti, L., Pizzella, V. & Zappasodi, F. Comparison of connectivity analyses for resting state eeg data. *Journal of Neural Engineering*. **14**(3), 036017 (2017).
37. Gómez-Ramírez, J., Freedman, S., Mateos, D., Pérez-Velázquez, J. L. & Valiente, T. Eyes closed or eyes open? exploring the alpha desynchronization hypothesis in resting state functional connectivity networks with intracranial eeg. (2017).
38. Han, J. et al. Eyes-open and eyes-closed resting state network connectivity differences. *Brain Sciences*. **13**(1), 122 (2023).
39. Smith, S. M. et al. Resting-state fmri in the human connectome project. *NeuroImage*. **80**, 144–168 (2013).
40. Barch, D. M. Resting-state functional connectivity in the human connectome project: current status and relevance to understanding psychopathology. *Harvard review of psychiatry*. **25**(5), 209–217 (2017).
41. Colclough, G. L. et al. How reliable are meg resting-state connectivity metrics?. *NeuroImage*. **138**, 284–293 (2016).
42. Soyuhos, O. & Baldauf, D. Functional connectivity fingerprints of the frontal eye field and inferior frontal junction suggest spatial versus nonspatial processing in the prefrontal cortex. *European Journal of Neuroscience*. **57**(7), 1114–1140 (2023).
43. Chen, J. E. et al. Resting-state “physiological networks”. *NeuroImage*. **213**, 116707 (2020).
44. Stam, C. J., Walsum, A.-M. v. C. & Micheloyannis, S. Variability of eeg synchronization during a working memory task in healthy subjects. *International Journal of Psychophysiology*. **46**(1), 53–66 (2002).
45. Sarnthein, J., Petsche, H., Rappelsberger, P., Shaw, G. L. & von Stein, A. Synchronization between prefrontal and posterior association cortex during human working memory. *Proceedings of the National Academy of Sciences*. **95**(12), 7092–7096 (1998).
46. Tallon-Baudry, C. Oscillatory synchrony in the monkey temporal lobe correlates with performance in a visual short-term memory task. *Cerebral Cortex*. **14**(7), 713–720 (2004).
47. Sanchez, J. M., Bornot, K. W., Ahmad, A. L. & Prasad, G. Robust eeg/meg based functional connectivity with the envelope of the imaginary coherence: Sensor space analysis. *Brain Topography*. **31**(6), 895–916 (2018).
48. Pascual-Marqui, R. D. et al. Assessing interactions in the brain with exact low-resolution electromagnetic tomography. *Philosophical Transactions of the Royal Society A: Mathematical, Physical and Engineering Sciences*. **369**(1952), 3768–3784 (2011).
49. Nunez, P. L. & Srinivasan, R. *Electric fields of the brain: the neurophysics of EEG* (Oxford University Press, USA, 2006).
50. Grech, R. et al. Review on solving the inverse problem in EEG source analysis. *Journal of NeuroEngineering and Rehabilitation*. **5**(1), (2008).
51. Acar, Z. A. & Makeig, S. Effects of forward model errors on eeg source localization. *Brain Topography*. **26**(3), 378–396 (2013).
52. Colclough, G. L., Brookes, M. J., Smith, S. M. & Woolrich, M. W. A symmetric multivariate leakage correction for meg connectomes. *NeuroImage*. **117**, 439–448 (2015).
53. Zokaie, N., & Husain, M. *Working Memory in Alzheimer's Disease and Parkinson's Disease*, page 325–344. Springer International Publishing, (2019).
54. Pijnenburg, Y. A. L. et al. EEG synchronization likelihood in mild cognitive impairment and alzheimer's disease during a working memory task. *Clinical Neurophysiology*. **115**(6), 1332–1339 (2004).

Author contributions

Narayan Puthanmadam Subramaniam and Tara C. Thiagarajan conceived the methodology. Narayan Puthanmadam Subramaniam implemented the methods, produced the results and prepared the visualizations. Narayan Puthanmadam Subramaniam and Tara C. Thiagarajan interpreted the results. Narayan Puthanmadam Subramaniam wrote the main manuscript. Tara Thiagarajan and Narayan Puthanmadam Subramaniam reviewed and edited the manuscript.

Declarations

Competing interests

The authors declare no competing interests.

Additional information

Supplementary Information The online version contains supplementary material available at <https://doi.org/10.1038/s41598-025-94076-0>.

Correspondence and requests for materials should be addressed to N.P.S.

Reprints and permissions information is available at www.nature.com/reprints.

Publisher's note Springer Nature remains neutral with regard to jurisdictional claims in published maps and institutional affiliations.

Open Access This article is licensed under a Creative Commons Attribution-NonCommercial-NoDerivatives 4.0 International License, which permits any non-commercial use, sharing, distribution and reproduction in any medium or format, as long as you give appropriate credit to the original author(s) and the source, provide a link to the Creative Commons licence, and indicate if you modified the licensed material. You do not have permission under this licence to share adapted material derived from this article or parts of it. The images or other third party material in this article are included in the article's Creative Commons licence, unless indicated otherwise in a credit line to the material. If material is not included in the article's Creative Commons licence and your intended use is not permitted by statutory regulation or exceeds the permitted use, you will need to obtain permission directly from the copyright holder. To view a copy of this licence, visit <http://creativecommons.org/licenses/by-nc-nd/4.0/>.

© The Author(s) 2025